

Distributed Lloyd-based algorithm for uncertainty-aware multi-robot under-canopy flocking

Manuel Boldrer, Vít Krátký, Viktor Walter, Martin Saska

Abstract—In this letter, we present a distributed algorithm for flocking in complex environments that operates at constant altitude, without explicit communication, no a priori information about the environment, and by using only on-board sensing and computation capabilities. We provide sufficient conditions to guarantee collision avoidance with obstacles and other robots without exceeding a desired maximum distance from a predefined set of neighbors (flocking or proximity maintenance constraint) during the mission. The proposed approach allows to operate in crowded scenarios and to explicitly deal with tracking errors and on-board sensing errors. The algorithm was verified through simulations with varying number of UAVs and also through numerous real-world experiments in a dense forest involving up to four UAVs.

Index Terms—Multi-robot systems, Distributed control, Lloyd-based algorithms.

Video—<https://mrs.fel.cvut.cz/rbl>

Github—<https://github.com/ctu-mrs/rbl>

I. INTRODUCTION

Over the past few decades, numerous applications have emerged for multi-robot systems, exhibiting their undisputed benefits in diverse fields. These applications span domains such as logistics, surveillance, environment monitoring, disaster response, search and rescue, and agriculture among others, demonstrating their versatility. For many of these applications, having a swarm of robots able to flock together towards a desired location can be highly beneficial, due to redundancies and parallelization. Depending on the environments where robots operate, the reliability or availability of explicit communication between robots may be compromised.

In this work, we propose a Lloyd-based algorithm that relies solely on on-board sensing. We have synthesized a distributed algorithm in which each robot safely reaches its desired position while maintaining proximity to its teammates in cluttered environments. We choose Lloyd algorithm as a base for our method as it enables seamless multi-robot coordination without requiring robots to share unobservable or global information, and its safety guarantees are not dependent on finely tuned parameters.

Our algorithm takes inspiration from the nature; just like flock of birds or a school of fish, the robots do not need a

Manuscript received: September, 3, 2025; Revised December, 4, 2025; Accepted February, 27, 2026.

Manuel Boldrer, Vít Krátký, Viktor Walter, and Martin Saska are with the Department of Cybernetics, Czech Technical University in Prague, Karlovo náměstí 13, 121 35 Prague 2, Czechia, {name.surname}@fel.cvut.cz.

This paper was recommended for publication by Editor Giuseppe Loianno upon evaluation of the Associate Editor and Reviewers' comments. This work was funded by the Czech Science Foundation (GAČR) under research project no. 23-07517S, by the European Union under the project Robotics and advanced industrial production (reg. no. CZ.02.01.01/00/22_008/0004590).



Figure 1: Deployment of the proposed algorithm in a real-world scenario with 3 UAVs navigating in a forest.

leader and each robot makes its own decisions based on relative information, without relying on explicit communication. We validate our approach through simulations and experiments in the forest (see Figure 1).

A. Related works

Prior literature provides a considerable amount of algorithms for distributed motion coordination of multiple robots, but only a few of them can manage to work in a cluttered environment by also imposing the flocking constraint. Among them, a smaller subset is devoted to applications in the field without relying on explicit communication between the robots.

To position our work within the state of the art, we consider the following features. *Distributed control*: each robot makes decisions on the basis of local information, which is obtained by relying only on on-board sensors. *Asynchronous control*: each robot makes decisions independently, in asynchronous fashion. *Without explicit communication*: the robots do not exchange time-dependent information such as future trajectories, current positions or velocities. Moreover, they do not rely on a common reference frame. *Safety*: collision and obstacle avoidance is guaranteed at any time. *Proximity maintenance*: the distance between robots is guaranteed to be below the set threshold on maximum distance. *Uncertainties*: the approach is robust to bounded tracking errors and bounded measurement uncertainties. *Cluttered and highly dense environments*: the algorithm can operate in cluttered environments such as a forest. *On-board localization*: the algorithm is verified in unknown environments relying only on on-board localization. *Experiments*: the algorithm is tested on real robotic platforms in unstructured environments. *Open source code*: the algorithm is open source.

In Table I, we report an overview of the most closely related algorithms in the literature. We mark with “×” if the algorithm does not implement the feature, “√” if it does,

Method	[1]	[2]	[3]	[4]	[5]	[6]	[7]	[8]	[9]	[10]	[11]	[12]	[13]	[14]	[15]	[16]	[17]	[18]	[19]	[20]	[21]	[22]	[23]	[24]	[25]	ours	
Distributed	✓	✓	○	○	○	✓	✓	✓	✓	✓	○	✓	✓	✓	✓	✓	✓	✓	✓	✓	○	✓	✓	×	✓	✓	
Asynchronous	✓	✓	○	○	○	✓	✓	×	✓	✓	×	✓	✓	✓	✓	✓	✓	✓	✓	×	×	✓	✓	×	✓	✓	
w/o Comm.	○	×	×	×	×	✓	✓	×	○	×	×	×	×	×	✓	×	✓	×	×	×	×	×	×	×	×	✓	
Safety	✓	✓	✓	✓	✓	○	○	○	✓	✓	✓	✓	○	○	○	○	○	○	○	○	○	○	○	○	○	○	✓
Uncertainties	○	○	○	○	○	○	○	○	○	○	○	○	○	○	○	○	○	○	○	○	○	○	○	○	○	○	✓
Prox. Maint.	×	✓	✓	×	○	○	○	○	×	×	×	○	○	○	○	○	○	○	○	○	○	○	○	○	○	○	✓
Clutt. Envir.	×	✓	✓	✓	✓	○	○	✓	✓	×	✓	✓	×	✓	×	✓	×	×	×	×	✓	✓	✓	✓	✓	✓	
On-board Loc.	×	×	✓	✓	✓	✓	✓	×	×	×	×	×	×	×	×	×	×	×	×	×	×	×	×	×	×	✓	
Experiments	✓	✓	✓	✓	✓	✓	✓	×	✓	✓	✓	○	✓	✓	✓	✓	✓	✓	✓	○	○	×	×	×	×	✓	
Open Source Code	✓	✓	✓	✓	✓	✓	✓	×	×	×	✓	×	×	×	×	×	✓	×	×	×	✓	✓	✓	✓	✓	✓	

Table I: List of state-of-the-art algorithms. We indicate with “×” if the algorithm does not implement the feature as described in Section I-A, “✓” if it does, and “○” if it does only partially.

and finally, “○” if it does but only partially. As shown in Table I, our algorithm is unmatched in fulfilling all the specified features of interest. In fact, with respect to [1], we included the proximity maintenance constraints, the ability to deal with cluttered environments, tracking errors and uncertainties, without relying on explicit communication, nor an external localization system. Despite [3], [4] proposing valid solutions to the problem, their main limitations are the requirement of a trajectory broadcasting network and the absence of account of proximity maintenance, tracking errors and uncertainties. Similarly, in [5] the robots need to broadcast information such as poses, velocities, poses covariance, and global extrinsic transformations. On the other hand, [6], [7], do not rely on an explicit communication network, but they exhibit degraded performance in crowded scenarios, lack of safety guarantees, proximity maintenance, and robustness to tracking errors and uncertainties. In [9], the authors present a distributed solution, which in theory does not rely on explicit communication and accounts for uncertainties. However, in the experiments they rely on motion capture measurements adding limited noise errors, which is reasonable only in structured environment (i.e., laboratory conditions). With respect to [2], [26], where the authors introduced the flocking behavior in the Lloyd-based framework, we do not impose the line-of-sight constraints, i.e., two robots are considered in the proximity if they are close enough. This allows to increase the robots mobility and also to not rely on explicit communication. In Table I, we report additional relevant state-of-the-art algorithms. Notably, all of them share limitations related to the use of an explicit communication network and/or to not account for safety, proximity maintenance and the uncertainties. Conversely, in our work, we provide a method which implements all the fore-mentioned features as well as a comprehensive rule for the selection of the algorithm’s parameters based on measurable quantities (e.g., tracking error, or covariance of state estimates), which is often an unclear or empirical process in the state-of-the-art algorithms.

B. Contribution and paper organization

Our contribution is threefold. First, we propose a novel algorithm for flocking control in dense cluttered environments. The key novelties lie in our use of an adaptive control strategy to compensate for tracking errors and measurement uncertainties, combined with Convex Weighted Voronoi Diagrams (CWVD) to enhance the performance in a dense forest scenarios. Second,

we provide sufficient conditions for safety and proximity maintenance in cluttered environments and in the presence of flocking constraints. Finally, we validate the algorithm in the forest, relying only on on-board sensors, i.e., Inertial Measurement Unit (IMU), 2-D Lidar, altitude sensor, and UVDAR system [27], without relying neither on an explicit communication network nor GNSS signals nor having a common reference frame.

II. PROBLEM DESCRIPTION

Let us denote the positions of the robots with $p = [p_1, \dots, p_N]^T$, where $p_i = [x_i, y_i]^T$ and the obstacle positions by $o = [o_1, \dots, o_{N_o}]^T$, $o_k = [x_k, y_k]^T$. The mission space is represented by $\mathcal{Q} \in \mathbb{R}^2$, the weighting function that assesses the weights of the points $q \in \mathcal{Q}$ is $\varphi_i(q) : \mathcal{Q} \rightarrow \mathbb{R}_+$, while δ_i and δ_k^o are the occupancy radius of the i -th robot and the k -th obstacle respectively. The problem that we aim to solve reads as follow:

Problem 1. *Let N be the number of robots in the swarm, let \mathcal{N}_i be the set of neighbors of the robot i , and $\tilde{\mathcal{N}}_i \subseteq \mathcal{N}_i$ the set of neighbors that has to remain in the proximity of the robot i for the entire mission. We want to synthesize a distributed control law, such that the swarm maintains the desired proximity constraints, which is characterized by a set of maximum distances $\Gamma = \{\Gamma_{ij} \mid i \in 1, \dots, N, j \in \tilde{\mathcal{N}}_i\}$. Each robot in the swarm has to reach its goal region avoiding collisions with other robots and obstacles.*

III. PROPOSED APPROACH

The presented approach is grounded in the Lloyd algorithm [28]. Let us consider the following cost function

$$J_{\text{cov}}(p, \mathcal{V}) = \sum_{i \in \mathcal{N}_i} \int_{\mathcal{V}_i} \|q - p_i\|^2 \varphi_i(q) dq, \quad (1)$$

where $\mathcal{V} = \{\mathcal{V}_1, \dots, \mathcal{V}_N\}$, $\mathcal{V}_i = \mathcal{V}_i^p \cap \mathcal{V}_i^o$ with \mathcal{V}_i^p being the i -th Convex Weighted Voronoi Diagram (CWVD) introduced in [12], which accounts only for neighboring robots’ positions, while \mathcal{V}_i^o is the i -th CWVD accounting only for neighboring obstacles’ positions:

$$\mathcal{V}_i^p = \{q \in \mathcal{Q} \mid w_i^x \cos \alpha_{ij} + w_i^y \sin \alpha_{ij} < \frac{1}{\epsilon_p} \|p_i - p_j\|, \quad (2) \\ \forall j \in \mathcal{N}_i\}.$$

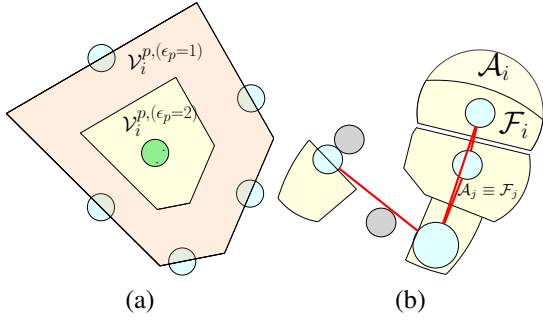


Figure 2: (a) Representation of the Convex Weighted Voronoi Diagram (CWVD) \mathcal{V}_i^p in (2) with $\epsilon_p = 2$ and $\epsilon_p = 1$. Where the green circle is the i -th robot and the cyan circles represent the neighboring robots. (b) Example of \mathcal{F}_i and \mathcal{A}_i cell geometry with $\epsilon_p = \epsilon_o = 2$. Red solid lines indicate the proximity maintenance constraints. Obstacles are represented as grey circles, while the robots are depicted in cyan.

$$\mathcal{V}_i^o = \{q \in \mathcal{Q} \mid w_i^x \cos \alpha_{ij} + w_i^y \sin \alpha_{ij} < \frac{1}{\epsilon_o} \|p_i - o_j\|, \quad \forall j \in \mathcal{O}_i\}, \quad (3)$$

where $w_i = [w_i^x, w_i^y]^\top = q - p_i$ and $\alpha_{ij} = \arctan\left(\frac{y_j - y_i}{x_j - x_i}\right)$, while $\epsilon_{p(o)} \in [1, 2]$ regulates the cautiousness in the robot motion (i.e., $\epsilon_{p(o)} = 1$ more aggressive behavior, $\epsilon_{p(o)} = 2$ more conservative behavior, notice that the latter coincides with the classic Voronoi diagram). In Figure 2a, we depict an example of the CWVD (2) for the case where $\epsilon_p = 2$ and $\epsilon_p = 1$.

By following the gradient descent of the cost function (1), we obtain the following proportional control law

$$\dot{p}_i(\mathcal{V}_i) = -k_{p,i}(p_i - c_{\mathcal{V}_i}), \quad (4)$$

where $k_{p,i} > 0$ is a positive real number, and

$$c_{\mathcal{V}_i} = \frac{\int_{\mathcal{V}_i} q \varphi_i(q) dq}{\int_{\mathcal{V}_i} \varphi_i(q) dq} \quad (5)$$

is the centroid position evaluated over the \mathcal{V}_i cell. By imposing (4), assuming a time-invariant $\varphi_i(q)$, each robot $i \in 1, \dots, N$, converges asymptotically to the centroid position $c_{\mathcal{V}_i}$ [29]. In the following, we show how we can attain a safe and effective algorithm for multi-robot swarming by introducing suitable modifications to the geometry of cell \mathcal{V}_i and crafting an appropriate weighting function $\varphi_i(q)$

A. Reshaping the cell geometry \mathcal{V}_i

The reshape of the cell geometry is both necessary and sufficient to ensure safety guarantees. Hence, we define the cell $\mathcal{A}_i = \tilde{\mathcal{V}}_i^p \cap \tilde{\mathcal{V}}_i^o \cap \mathcal{S}_i$, where

$$\tilde{\mathcal{V}}_i^p = \begin{cases} \mathcal{V}_i^p & \text{if } \frac{1}{2} \|p_i - p_j\| > \Delta_{ij}, \forall j \in \mathcal{N}_i, \\ \{q \in \mathcal{Q} \mid \|q - p_i\| \leq \|q - \tilde{p}_j\|, \forall j \in \mathcal{N}_i\} & \text{otherwise,} \end{cases} \quad (6)$$

where $\Delta_{ij} = \delta_j + \delta_i$, and $\tilde{p}_j = p_j + 2\left(\Delta_{ij} - \frac{\|p_i - p_j\|}{2}\right) \frac{p_i - p_j}{\|p_i - p_j\|}$, takes into consideration the physical dimension of the robots. To account for the obstacles,

$$\tilde{\mathcal{V}}_i^o = \begin{cases} \mathcal{V}_i^o & \text{if } \frac{1}{2} \|p_i - p_j\| > \Delta_{ij}^o, \forall j \in \mathcal{O}_i, \\ \{q \in \mathcal{Q} \mid \|q - p_i\| \leq \|q - \tilde{o}_j\|, \forall j \in \mathcal{O}_i\} & \text{otherwise,} \end{cases} \quad (7)$$

where $\Delta_{ij}^o = \delta_i + \delta_j^o$ and $\tilde{o}_j = o_j + 2\left(\Delta_{ij}^o - \frac{\|p_i - o_j\|}{2}\right) \frac{p_i - o_j}{\|p_i - o_j\|}$, takes into consideration the size of the robot and the obstacles, while

$$\mathcal{S}_i = \{q \in \mathcal{Q} \mid \|q - p_i\| \leq r_{s,i}\}, \quad (8)$$

where $r_{s,i}$ is half of the sensing radius R_s of the robot i .

Theorem 1 (Safety). *By imposing the control $\dot{p}_i(\mathcal{A}_i)$ in (4), with $\mathcal{A}_i = \tilde{\mathcal{V}}_i^p \cap \tilde{\mathcal{V}}_i^o \cap \mathcal{S}_i$, collision avoidance is guaranteed at every instant of time.*

Proof. The proof comes from the definition of convex set. Due to the fact that the set \mathcal{A}_i is always convex, and by definition $p_i, c_{\mathcal{A}_i} \in \mathcal{A}_i$, it follows that since the straight path from the robot position to the centroid position is a safe path, then applying $\dot{p}_i(\mathcal{A}_i)$ in (4) preserves safety. Due to the robots' size, the condition that the straight path from the robot to its centroid position is a safe path can be violated only if the i -th robot is at a distance greater than $2\Delta_{ij}$ ($2\Delta_{ij}^o$) from the j -th robot (j -th obstacle), according to (6), (7). Nevertheless, to experience collision the distance between the i -th robot and the j -th robot (j -th obstacle) needs to be less than $2\Delta_{ij}$ ($2\Delta_{ij}^o$), i.e., equal to Δ_{ij} (Δ_{ij}^o), hence safety is preserved. \square

We further apply an additional reshaping of the cell geometry in order to maintain the desired proximity of the agents, i.e., to achieve flocking behavior. By imposing our final cell geometry $\mathcal{F}_i = \mathcal{A}_i \cap \mathcal{M}_i$, where

$$\mathcal{M}_i = \{q \in \mathcal{Q} \mid \|q - p_j\| \leq \Gamma_{ij}, \forall j \in \tilde{\mathcal{N}}_i\}, \quad (9)$$

we obtain proximity maintenance while preserving safety. In Figure 2b, we depict an example of cell geometry \mathcal{F}_i .

Theorem 2 (Proximity maintenance or flocking constraint). *By imposing the control $\dot{p}_i(\mathcal{F}_i)$ in (4), both safety and proximity maintenance are guaranteed at every instant of time.*

Proof. Given that $\mathcal{F}_i \subseteq \mathcal{A}_i$, safety comes from Theorem 1. Since \mathcal{M}_i is convex by definition, \mathcal{F}_i is also convex, and thus the centroid $c_{\mathcal{F}_i} \in \mathcal{F}_i$. It implies that by imposing $\dot{p}_i(\mathcal{F}_i)$ in (4), $p_i \in \mathcal{F}_i$ at any time. Hence, by the definition of the \mathcal{F}_i set, proximity maintenance between i and j is always preserved. \square

B. The weighting function $\varphi_i(q)$

Although ensuring safety and proximity maintenance only involves properly shaping the cell geometry, convergence to the goal and enhancing navigation performance largely hinges on how the function $\varphi_i(q)$ is defined. As originally proposed in [1], we adopt a Laplacian-shaped function centered at \bar{p}_i , which represents a point in the mission space that ultimately needs to converge to the goal location. We design the $\varphi_i(q)$ function as follows:

$$\varphi_i(q) = \exp\left(-\frac{\|q - \bar{p}_i\|}{\beta_i}\right), \quad (10)$$

where the spreading factor $\beta_i \in \mathbb{R}$ is time-variant. It follows the dynamics

$$\dot{\beta}_i(\mathcal{A}_i) = \begin{cases} -k_\beta \beta_i & \text{if } \|c_{\mathcal{A}_i} - p_i\| < d_1 \wedge \\ & \|c_{\mathcal{A}_i} - c_{\mathcal{S}_i}\| > d_2, \\ -k_\beta(\beta_i - \beta_i^D) & \text{otherwise,} \end{cases} \quad (11)$$

and

$$\begin{aligned} \dot{\bar{p}}_i &= \begin{cases} -k_e(\bar{p}_i - R(\pi/2 - \varepsilon)e_i) & \text{if } \|c_{\mathcal{A}_i} - p_i\| < d_3 \wedge \\ & \|c_{\mathcal{A}_i} - c_{\mathcal{S}_i}\| > d_4, \\ -k_e(\bar{p}_i - e_i) & \text{otherwise,} \end{cases} \\ \bar{p}_i &= e_i \text{ if } \|p_i - \bar{c}_{\mathcal{A}_i}\| > \|p_i - c_{\mathcal{A}_i}\| \wedge \bar{p}_i = R(\pi/2 - \varepsilon)e_i. \end{aligned} \quad (12)$$

The parameters $\beta_i^D, d_1, d_2, d_3, d_4, k_\beta, k_e$ are positive scalars, $R(\theta)$ is the rotation matrix, e_i is the goal position for the i -th robot, ε is a small number, which allows to avoid rotations equal to $\pi/2$, while $\bar{c}_{\mathcal{A}_i}$ is the centroid position computed over the cell \mathcal{A}_i with $\bar{p}_i \equiv e_i$. Equations (11) and (12) specify two adaptive rules. Intuitively, (11) regulates the greediness of the robot i in reaching its goal region, while (12) introduces a right (or left) hand-side rule to enforce a common behavioral convention across the robots and hence enhance inter-robot coordination.

C. Dealing with dynamics and uncertainties

The robot deployment requires to consider a set of additional issues. First, more complex dynamics of the robots must be applied as $\dot{p}_i = u_i$ is not directly applicable. As a consequence, tracking error, which is caused by model mismatch and external disturbances, generating a difference between the desired and the actual velocity, has to be taken into account. Finally, we have to consider measurement uncertainties arising from limitations of the perception system providing an estimate of the positions of other robots and obstacles with a certain error.

To account for the dynamic constraints of the robots, we synthesize the control inputs through an MPC formulation (similarly to [1], [9]). Hence, each robot i solves the following optimization problem (for the sake of clarity we discard the i indexing),

$$\text{minimize}_{x_k, u_k} \sum_{k=0}^{N_t} J(x_k, u_k, c_{\mathcal{F}}), \quad (13a)$$

$$\text{s.t.: } x_k = f(x_{k-1}, u_{k-1}), \quad \forall k \in (1, N_t), \quad (13b)$$

$$x_k \in \mathcal{X}, u_k \in \mathcal{U}, \quad \forall k \in (0, N_t), \quad (13c)$$

$$x_0 = x_{\text{init}}, \quad (13d)$$

where k indicates the time index, N_t indicates the horizon length, J represents the cost function, $x_k = [p_k^\top, \dot{p}_k^\top, \ddot{p}_k^\top]^\top$ and u_k are the state and control inputs respectively, $f(x_{k-1}, u_{k-1})$ indicates the dynamics of the robot, $x_k \in \mathcal{X}$, $u_k \in \mathcal{U}$ are the state and input constraints respectively, and $x_0 = x_{\text{init}}$ is the initial condition.

Both the tracking errors and measurement uncertainties can be accounted for by means of an adaptive strategy. Specifically, it is achieved by adapting the value of β_i in (11) in an online fashion. An alternative approach would be reshaping the \mathcal{F}_i cell, similarly to [9]. However, this method cannot be applied in our case, since, by following this approach, the robot may fall out of its cell due to tracking error, and once it happens, both the cell and the centroid position are no longer defined. Conversely, the value of β_i defines the aggressiveness of the i -th robot. A smaller value corresponds to a centroid position

closer to the goal (and hence closer to the boundaries of the \mathcal{F}_i cell, namely $\partial\mathcal{F}_i$), while larger values of β_i push the centroid position as far as possible from the boundaries of the cell $\partial\mathcal{F}_i$. Thus, managing errors and uncertainties is achieved by selecting a value of β_i such that the centroid position stays at a controlled distance from the boundary of the cell. This distance must be chosen in accordance with the maximum positional tracking error and the maximum error in the neighbors' position estimates. More formally, it can be done by imposing a lower bound to β_i in (11) equal to

$$\beta_i^{\min} = \arg \min_{\beta_i} (\|c_{\mathcal{F}_i} - p_{\partial\mathcal{F}_i}\| - d_u)^2, \quad (14)$$

where $p_{\partial\mathcal{F}_i}$ is the position of the closest point to $c_{\mathcal{F}_i}$ on the boundary of \mathcal{F}_i , while d_u is a threshold value that has to be tuned on the basis of the tracking errors and measurement uncertainties. For the sake of clarity, we depicted three scenarios in Figure 3. Figure 3a considers the tracking error; in this case the value of $c_{\mathcal{F}_i}$ is controlled to stay at least at a distance d_u^t from the boundary $\partial\mathcal{F}_i$. We indicate with \mathcal{Z}_i the region set where the i -th robot is allowed to go in the next time step. Notice that the dimension of the region \mathcal{Z}_i can be controlled by d_u^t . To be conservative, the value of d_u^t should be determined empirically as the maximum tracking error, and it can be set as a function of the velocity. In Figure 3b, we show the case where we have measurement uncertainties. We illustrate both the i -th and the j -th robots' positions and the ellipse of uncertainty $\mathcal{E}_{i,j}$. In this case, \mathcal{K}_i indicates the region where the centroid $c_{\mathcal{F}_i}$ has to be constrained to preserve safety. Let us consider the case where $\epsilon_{p(o)} = 1$. By relying on geometric reasoning (refer to Figure 3b), depending on the inter-robot distance measurement uncertainty, we can select the parameter d_u^m as

$$d_u^m \geq k\sqrt{\lambda^{\max}} + \delta_j + \delta_i, \quad (15)$$

where λ^{\max} is the maximum eigenvalue of the covariance matrix associated with the distance measurement and k is a scale factor that defines the confidence ellipse.

From a practical point of view, the value of d_u^m may be set empirically to a constant that satisfies inequality (15) in the worst expected scenario. In real-world equipments the uncertainties associated with the measurements are far from being constant values. Hence, the user can set d_u^m dynamically, based on the current measurement uncertainties, which are reported by the equipment together with the measurement means. One method to implement this, is to use the *restraining* method from [30]. This technique offsets the set-points of the robots from an ideal target location according to the probability distributions of relative pose observations.

On the other hand, to preserve proximity maintenance, a sufficient condition is that $d_u^m \geq k\sqrt{\lambda^{\max}}$. Finally, the tracking error and measurement uncertainties are combined as $d_u = d_u^m + d_u^t$ in Figure 3c.

Hence, by imposing the control $\dot{p}_i(\mathcal{F}_i)$ in (4), with $\mathcal{F}_i = \tilde{\mathcal{V}}_i^p \cap \tilde{\mathcal{V}}_i^o \cap \mathcal{S}_i \cap \mathcal{M}_i$ and assuming a maximum uncertainty in the estimation of the other robots' distances equal to $k\sqrt{\lambda^{\max}}$, by selecting $d_u^m \geq k\sqrt{\lambda^{\max}}$, and assuming a bounded maximum tracking error less or equal than d_u^t , both safety and proximity maintenance are preserved by selecting β_i^{\min} according to (14)

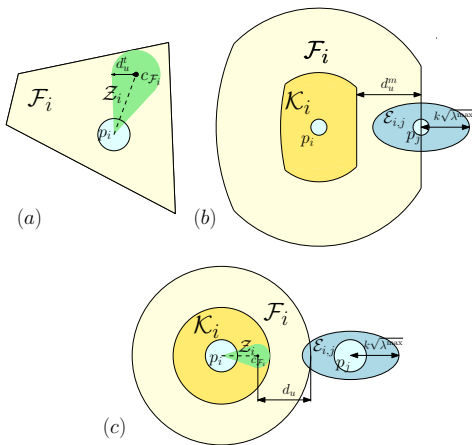


Figure 3: Dealing with uncertainties: (a) tracking error case, (b) measurement uncertainty case, (c) combined tracking error and measurement uncertainty. The robots are indicated with the cyan circles. We represent in light yellow the \mathcal{F}_i set, in dark yellow the set \mathcal{K}_i , in green the set \mathcal{Z}_i , in blue the ellipse of uncertainty $\mathcal{E}_{i,j}$.

for all $i = 1, \dots, N$. Specifically, let us choose d_u^m such that it satisfies (15) and $d_u = d_u^t + d_u^m$. By enforcing a lower bound β_i^{\min} (14), we set a minimum distance d_u between the centroid position $c_{\mathcal{F}_i}$ and the boundary of the cell $\partial\mathcal{F}_i$. Due to the definition of d_u , this margin explicitly accounts for both estimation uncertainty and tracking error, thereby ensuring safety and proximity maintenance for all admissible realizations of the neighbors' positions within the confidence ellipse. More intuitively, the centroid is constrained to remain within a region that preserves safety and proximity maintenance by accounting for tracking error and all possible neighbors' positions consistent with the uncertainty bounds. If there exists no point $q \in \mathcal{F}_i$ such that $\text{dist}(q, \partial\mathcal{F}_i) \geq d_u$, according to (14), the centroid position $c_{\mathcal{F}_i}$ is the point that maximizes the distance from $\partial\mathcal{F}_i$. Under this condition, strict guarantees of safety and proximity maintenance cannot be ensured for all possible uncertainty realizations. Nevertheless, in this case the robot adopts the most conservative behavior, placing the centroid at the location that maximizes boundary clearance. The guarantees provided by the proposed conditions are therefore sufficient and hold whenever a feasible margin exists; they rely on worst-case realizations within the assumed uncertainty bounds and bounded tracking errors.

Remark 1 (Tracking error and measurement uncertainties invariance property). *Since we are adopting the same strategy to account for the tracking errors and measurements uncertainty, we get the property of invariance. In practice, it does not matter how d_u^m and d_u^t are chosen, what matters is the sum d_u , hence in the case of underestimation of one of the two terms, it is compensated by the other.*

IV. SIMULATION RESULTS

In this section, we first show through simulations the scalability, repeatability and robustness of our approach in two different scenarios, with and without accounting for uncertainties and tracking errors. Then we report a comparison with PACNav [6], the algorithm does not rely on communication network, and shares similar features with the proposed algorithm (refer to

N	$d_u = 0$ (m)		$d_u = 1.0$ (m)	
	avg. time (s)	SR	avg. time (s)	SR
9	32.71	0.50	54.91	1.00
16	34.94	0.40	64.53	1.00

Table II: The simulation results obtained in terms of time to reach the goal and success rate (SR) for 10 instances in 2 different scenarios with $N = [9, 16]$. We report the results with different parameter selection i.e., $d_u = 0$ (m) and $d_u = 1.0$ (m).

Table I). Notice that comparing with algorithm such as [3]–[5] is out of scope of this paper. In most of the scenarios, our method does not perform better than algorithms that can share information, such as future trajectories, among the robots. Despite [6] performs well in relatively simple environments and with a limited number of robots, it lacks reliability in more complex scenarios. In addition, crucial requirements such as safety and proximity maintenance depend strongly on fine parameter tuning. This is a common issue in the state-of-the-art algorithms, which is overcome in our solution, where the parameter selection affects only the performance of the mission, while, safety and proximity maintenance are met if they are selected according to the theoretical findings. All the simulations are performed by relying on the MRS simulator [31], which account for full rigid-body UAV dynamics.

In the first simulations, we consider different set of parameters $d_u = [0, 1.0]$ (m) in two different scenarios, with $N = [9, 16]$, $\delta_i = 0.2$ (m), $\epsilon = 1.0$, and randomly generated circular obstacles with $\delta_o = 0.15$ (m) (see Figure 4). We select the parameters as follows for all the simulations $r_{s,i} = 5.0$ (m), $d_1 = d_2 = d_3 = d_4 = 1$ (m), $\beta_i^D = 0.15$, $\Gamma_{ij} = 10$ (m), while the adjacency matrices defining proximity maintenance constraints are defined as grid matrices, as depicted in Figure 4 (red lines). We simulated UVDAR noise as a bounded radial random measurement error with magnitude not exceeding 0.8 (m). In Table II, we report the quantitative results in terms of average time to reach the goal and success rate over a total of 40 runs. As expected, setting $d_u = 0$ (m) leads to better performance in terms of time to reach the goal; however, it does not ensure collision avoidance between the robots. In contrast, selecting d_u according to the theoretical findings results in safe behavior and preserves the proximity maintenance constraints. Figure 4 illustrates the two scenarios with $N = [9, 16]$ robots, and shows the trajectories generated for one instance with $d_u = 1.0$ (m). Figure 5 illustrates the distance between each robot in the two scenarios. The colored lines indicate whether the proximity maintenance constraint is active. To further validate the robustness of the proposed approach, we additionally performed 200 simulations across four different parameter sets in the same scenario depicted in Figure 4a, consistently achieving the goal preserving safety and the proximity maintenance constraints.

For the comparison with PACNav [6], we simulate three scenarios with different number of robots and a varying number of randomly generated circular obstacles. In the simulation, we do not inject noise in the measurements, nevertheless tracking error is present. For each scenario, we perform 10 runs for statistical evidence. The metrics that we took into account

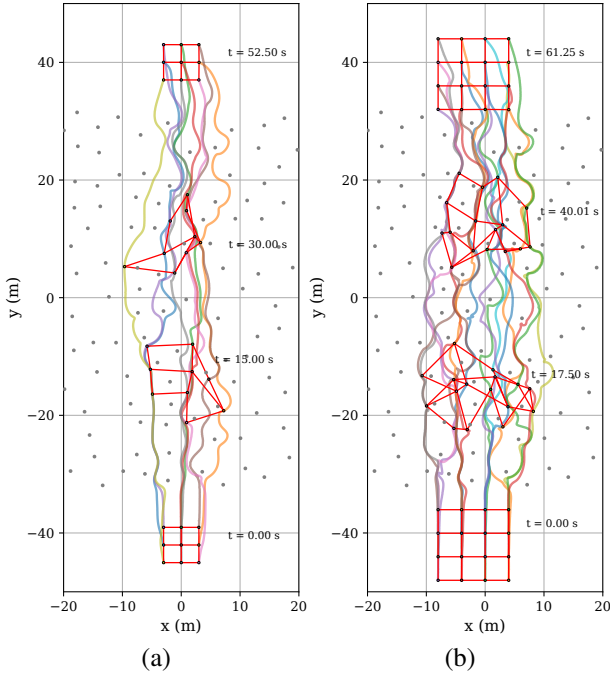


Figure 4: Simulation results with $N = 9$ and $N = 16$ robots, with $d_u = 1.0$ (m). The images represent example scenarios used for generation of results presented in Table II. Colored circles represent the robots' positions at different time t . Red lines represent the proximity maintenance constraints between the robots. Black dots are the obstacles in the scene.

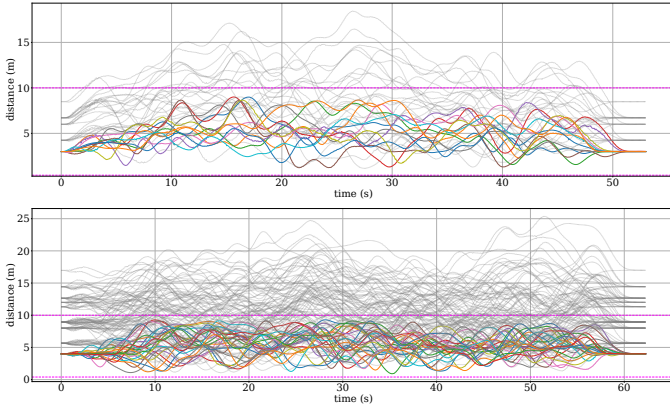


Figure 5: Distances between UAVs in the simulations in Figure 4a and 4b. The flocking and safety constraints are in magenta. Colored lines indicate the presence of an active flocking constraint between the two robots.

are the time required for all the robots to travel 42 meters in the goal direction and the success rate in terms of mutual collision avoidance and obstacle avoidance. In Table III, we report the results obtained from PACNav [6] and from our approach. We considered the following scenarios: $N = [4, 9, 9]$, $\delta_i = [0.25, 0.5, 0.5]$ (m), $\delta_o = [0.3, 0.75, 0.75]$ (m), and we select the parameters as follows for all the three scenarios $r_{s,i} = 4.5$ (m), $d_1 = d_3 = 0.5$ (m), $d_2 = d_4 = 1$ (m), $\beta_i^D = 0.5$, $\Gamma_{ij} = 8$ (m), $d_u = 0.8$ (m). The adjacency matrices defining the proximity maintenance constraints were selected as grid adjacency matrices.

For our approach, we considered two different values for

Scenario	N	PACNav [6]		Our ($\epsilon = 2.00$)		Our ($\epsilon = 1.052$)	
		avg. time (s)	SR	avg. time (s)	SR	avg. time (s)	SR
1	3	55.01	1.00	39.96	1.00	24.23	1.00
2	9	-	0.00	45.71	1.00	29.53	1.00
3	9	-	0.00	120.33	1.00	55.87	1.00

Table III: The simulation results obtained in terms of time to reach the goal and success rate for 10 instances in 3 different scenarios, comparing PACNav [6] with our method in two different parameter configurations.

the parameters $\epsilon = \epsilon_p = \epsilon_o$. The parameter selection for PACNav [6] has been done by trial and error approach, on the basis of the environment and the number of robots. Besides that, as seen in Table III, PACNav does not scale in terms of performance (convergence, safety, and proximity maintenance) when the number of robots grows, due to the complex superimposition of forces given by the surroundings.

For further simulation results, please refer to the multimedia material.

V. EXPERIMENTAL RESULTS

To validate our algorithm, we implemented it on real robotic platforms. To detect the surrounding obstacles we relied on the RPLiDAR A3. In order to have a robust and safer perception system, we introduced a double layer of obstacles. The first layer of obstacles is given by the occupancy map built online by Hector [32], while the second layer is given by the raw pointcloud provided by the RPLiDAR A3. Given this information, we cluster the points on the basis of their spatial distribution. Then we compute the closest point to the robot position for each cluster, in order to estimate the position of the obstacles in the scene. By doing that, we exploit both the reactivity of the raw data coming from the LiDAR pointcloud, and at the same time, the scan-matching based obstacle representation, which is provided by the Hector mapping algorithm. At the same time we do not need to know the obstacles' size, since we are considering the closest point, we can account for a small value for δ^o . The relative positions of the neighboring robots are obtained by relying on the UltraViolet Direction And Ranging (UVDAR) technology [27]. The sensor system operates by detection of blinking ultraviolet LEDs. The blinking signal is retrieved by on-board cameras with tailored filters. Each UAV is individually identifiable according to its blinking frequency. The pose of the UAVs is inferred through computer vision techniques.

The experimental deployment is conducted in the forest, where we do not have access to the GNSS signal. The goal positions are set to be 40 (m) ahead with respect to the initial position of each robot, notice that we do not need to have a common reference frame. We choose to adopt a fixed value of d_u in the experiments. Due to the high measurements' uncertainties the value of d_u did not satisfy (15) all the time. In this regard, two practical solutions were adopted in the experiments: (i) We discard measurements with values of $\lambda^{\max} > 15$, and (ii) if the measured distance between i -th and j -th robot with $j \in \mathcal{N}_i$ is greater than Γ_{ij} , we re-project the position of the j -th robot to be at a distance less than Γ_{ij} from the i -th robot, in order to ensure the existence of a nonempty set \mathcal{F}_i . These two strategies help to practically

UAV	UAV1	UAV2	UAV3	UAV4
avg. speed (m/s)	0.361	0.329	0.373	0.370
max. speed (m/s)	1.256	1.224	1.427	1.095
time (s)	150.61	174.95	159.20	174.20

Table IV: Average speed, maximum speed, and time to reach the goal of each UAV in the experiment from Figure 6.

manage large estimation errors that exceed the theoretical threshold e.g., temporary failures in the estimation of distance to other robot's due to tree occlusions.

We tested the algorithm with up to $N = 4$, by selecting $\delta_i = 0.3$ (m), $\delta^o = 0.05$ (m), $r_{s,i} = 6$ (m), $d_1 = d_3 = 0.5$ (m), $d_2 = d_4 = 1$ (m), $\beta_i^D = 2.5$, $\Gamma_{ij} = 12$ (m), $d_u = 0.8$ (m), $\epsilon_p = \epsilon_o = 1.052$, and the adjacency matrix that defines the flocking constraints is $A_d = \begin{bmatrix} 0 & 1 & 0 & 1 \\ 1 & 0 & 1 & 0 \\ 0 & 1 & 0 & 1 \\ 1 & 0 & 1 & 0 \end{bmatrix}$.

In Figure 6-(a) we show the trajectory of UAV 2, the positions of the other robots measured by UVDAR system, and the map built by UAV 2 by using Hector SLAM during the mission. In Figure 7, we depict the distances between UAV 2 and the other robots according to the UVDAR measurements. In Table IV, we report the average velocities, the maximum velocities, and the time to reach the goal for each UAV during the mission. To verify the success of the mission, we report in Figure 6-(b) the actual trajectories for all the 4 robots in the mission, while in Figure 8 we show the distances between the UAVs during the mission. The safety constraints and the flocking constraints (according to the adjacency matrix A_d) were satisfied during the entire mission.

To show reliability and robustness to parameter changes, we report in Table V the results obtained from other four experiments in the forest, with $N = 3$ UAVs. Since the system is intrinsically chaotic it does not make sense to compare the results obtained, even if, as we can expect, a relation between β^D and the time to reach the goal can be inspected from Table V. Nevertheless, through the table we want to show the repeatability of the experiments and the robustness to parameter changes. The parameters for each experiment were set as follows: #experiment = [1, 2, 3, 4], $N = [3, 3, 3, 3]$, $\delta_i = [0.3, 0.3, 0.3, 0.3]$ (m), $\delta^o = [0.05, 0.05, 0.05, 0.05]$ (m), $r_{s,i} = [6, 6, 6, 6]$ (m), $d_1 = d_3 = [0.5, 0.5, 0.5, 0.5]$ (m), $d_2 = d_4 = [1, 1, 1, 1]$ (m), $\beta_i^D = [2.0, 2.0, 1.0, 0.6]$, $\Gamma_{ij} = [12, 10, 10, 10]$ (m), $d_u = [0.75, 0.75, 0.75, 0.75]$ (m), $\epsilon_p = \epsilon_o = [1.052, 1.052, 1.010, 1.052]$, and the adjacency matrix that defines the flocking constraints is the same for all the four experiments, $A_d = \begin{bmatrix} 0 & 0 & 1 \\ 0 & 0 & 1 \\ 1 & 1 & 0 \end{bmatrix}$.

The videos of the experiments discussed in this section can be found in the multimedia material.

VI. CONCLUSIONS

In this paper, we presented a novel distributed algorithm to swarm reliably and effectively in dense cluttered environments represented by a forest. We provide sufficient conditions for safety and proximity maintenance. We propose an adaptive strategy to compensate for tracking errors and measurement uncertainties. We compare our approach with state-of-the-art algorithms, and finally we validate our solution through simulations and experiments in the field and in dense environment

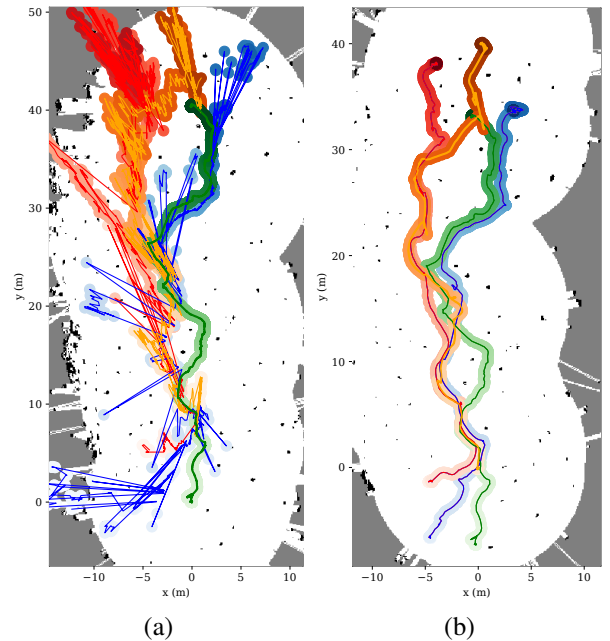


Figure 6: Experiment in the forest. In (a) the trajectory of UAV 2 is depicted in green. The positions measured through UVDAR by UAV 2 are depicted in orange (UAV 1), blue (UAV 3), and red (UAV 4). The map built by UAV 2 by means of Hector mapping is also represented, in particular the free space is white, obstacles are black and the unexplored area is grey. In (b) we depicted the actual trajectories obtained in post-process phase through transformation of odometries to a common reference frame. The map was built by UAV 1.

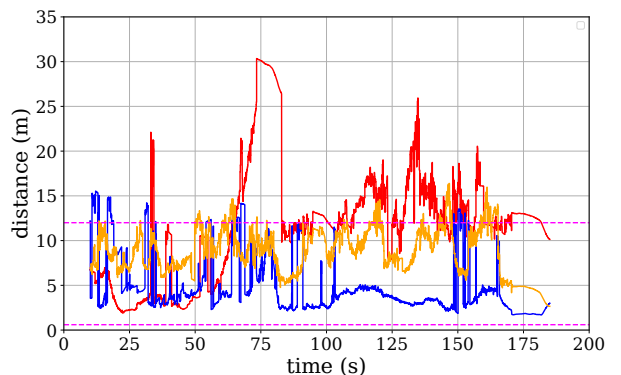


Figure 7: Distances measured by UVDAR system on UAV 2 from UAV 1 (blue), UAV 3 (orange), and UAV 4 (red). The flocking and safety constraints are in magenta.

such as a forest. Our approach presents some limitations; the algorithm is limited to work on a plane, i.e., the reference in the altitude for each robot is constant and equal. The convergence towards the goal depends on both the environment of operation and the uncertainties taken into account. Providing to the algorithm a higher level re-planner can be beneficial to enhance performance. Future research directions will be focused on an effective 3D extension of the Lloyd algorithm and to further increase the agility of the swarm.

REFERENCES

- [1] M. Boldrer, A. Serra-Gomez, L. Lyons, V. Krátký, J. Alonso-Mora, and L. Ferranti, "Rule-based lloyd algorithm for multi-robot motion planning and control with safety and convergence guarantees," *arXiv preprint*

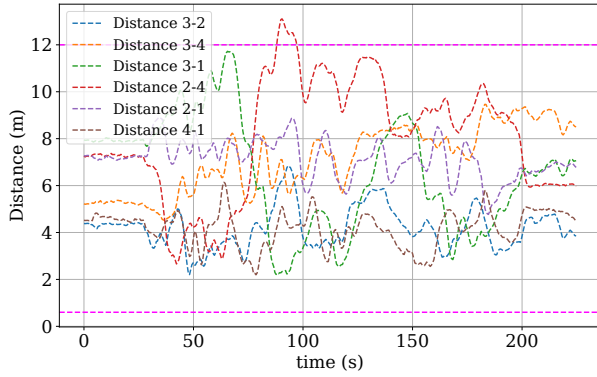


Figure 8: Distances between UAVs computed based on odometries transformed to a common reference frame obtained through alignment of maps of individual UAVs in a post-processing phase. The flocking and safety constraints are in magenta. According to A_d the flocking constraints are not active for the pair of robots 2-4 and 1-3.

	UAV1	UAV2	UAV3
Exp. 1 ($\beta^D = 2.0$, $\epsilon_{o(p)} = 1.052$, $\Gamma_{ij} = 12$)			
avg. speed (m/s)	0.309	0.249	0.263
max. speed (m/s)	1.210	1.255	1.226
time (s)	278.43	280.54	245.12
Exp. 2 ($\beta^D = 2.0$, $\epsilon_{o(p)} = 1.052$, $\Gamma_{ij} = 10$)			
avg. speed (m/s)	0.447	0.415	0.382
max. speed (m/s)	1.150	1.170	1.230
time (s)	148.00	163.81	159.91
Exp. 3 ($\beta^D = 1.0$, $\epsilon_{o(p)} = 1.010$, $\Gamma_{ij} = 10$)			
avg. speed (m/s)	0.661	0.497	0.740
max. speed (m/s)	1.229	1.245	1.374
time (s)	85.16	117.16	79.20
Exp. 4 ($\beta^D = 0.6$, $\epsilon_{o(p)} = 1.052$, $\Gamma_{ij} = 10$)			
avg. speed (m/s)	0.605	0.651	0.794
max. speed (m/s)	1.175	1.281	1.310
time (s)	82.49	80.33	62.30

Table V: Comparison of average speed, maximum speed, and time to reach the goal in four different experiments in the forest, showing repeatability and robustness to parameters changes.

arXiv:2310.19511, 2024.

[2] M. Boldrer, L. Palopoli, and D. Fontanelli, "A unified lloyd-based framework for multi-agent collective behaviours," *Robotics and Autonomous Systems*, vol. 156, p. 104207, 2022.

[3] X. Zhou, X. Wen, Z. Wang, Y. Gao, H. Li, Q. Wang, T. Yang, H. Lu, Y. Cao, C. Xu, et al., "Swarm of micro flying robots in the wild," *Science Robotics*, vol. 7, no. 66, p. eabm5954, 2022.

[4] X. Zhou, J. Zhu, H. Zhou, C. Xu, and F. Gao, "Ego-swarm: A fully autonomous and decentralized quadrotor swarm system in cluttered environments," in *2021 IEEE international conference on robotics and automation (ICRA)*, 2021, pp. 4101–4107.

[5] F. Zhu, Y. Ren, L. Yin, F. Kong, Q. Liu, R. Xue, W. Liu, Y. Cai, G. Lu, H. Li, and F. Zhang, "Swarm-lio2: Decentralized efficient lidar-inertial odometry for aerial swarm systems," *IEEE Transactions on Robotics*, vol. 41, pp. 960–981, 2025.

[6] A. Ahmad et al., "Pacnav: a collective navigation approach for uav swarms deprived of communication and external localization," *Bioin. & Biomim.*, vol. 17, no. 6, p. 066019, 2022.

[7] P. Petráček, V. Walter, T. Bača, and M. Saska, "Bio-inspired compact swarms of unmanned aerial vehicles without communication and external localization," *Bioin. & Biomim.*, vol. 16, no. 2, p. 026009, 2020.

[8] M. Boldrer, L. Palopoli, and D. Fontanelli, "Socially-aware multi-agent velocity obstacle based navigation for nonholonomic vehicles," in *2020 IEEE 44th Annual Computers, Software, and Applications Conference (COMPSAC)*. IEEE, 2020, pp. 18–25.

[9] H. Zhu, B. Brito, and J. Alonso-Mora, "Decentralized probabilistic multi-robot collision avoidance using buffered uncertainty-aware voronoi cells," *Autonomous Robots*, vol. 46, no. 2, pp. 401–420, 2022.

[10] L. Ferranti, L. Lyons, R. R. Negenborn, T. Keviczky, and J. Alonso-Mora, "Distributed nonlinear trajectory optimization for multi-robot motion planning," *IEEE Transactions on Control Systems Technology*, vol. 31, no. 2, pp. 809–824, 2022.

[11] V. K. Adajania, S. Zhou, A. K. Singh, and A. P. Schoellig, "Amswarm: An alternating minimization approach for safe motion planning of quadrotor swarms in cluttered environments," in *2023 IEEE International Conference on Robotics and Automation*, 2023, pp. 1421–1427.

[12] M. Boldrer, L. Palopoli, and D. Fontanelli, "Lloyd-based approach for robots navigation in human-shared environments," in *2020 IEEE/RSJ Intern. Conf. on Intell. Robots and Systems (IROS)*, 2020, pp. 6982–6989.

[13] G. Vásárhelyi, C. Virágh, G. Somorjai, N. Tarcai, T. Szörényi, T. Nepusz, and T. Vicsek, "Outdoor flocking and formation flight with autonomous aerial robots," in *2014 IEEE/RSJ International Conference on Intelligent Robots and Systems*, 2014, pp. 3866–3873.

[14] G. Vásárhelyi, C. Virágh, G. Somorjai, T. Nepusz, A. E. Eiben, and T. Vicsek, "Optimized flocking of autonomous drones in confined environments," *Science Robotics*, vol. 3, no. 20, p. eaat3536, 2018.

[15] J. M. Soares, A. P. Aguiar, A. M. Pascoal, and A. Martinoli, "A distributed formation-based odor source localization algorithm—design, implementation, and wind tunnel evaluation," in *IEEE International Conference on Robotics and Automation*, 2015, pp. 1830–1836.

[16] A. Wasik, J. N. Pereira, R. Ventura, P. U. Lima, and A. Martinoli, "Graph-based distributed control for adaptive multi-robot patrolling through local formation transformation," in *IEEE/RSJ International Conference on Intelligent Robots and Systems*, 2016, pp. 1721–1728.

[17] D. Mezey, R. Bastien, Y. Zheng, N. McKee, D. Stoll, H. Hamann, and P. Romanczuk, "Purely vision-based collective movement of robots," *npj Robotics*, vol. 3, no. 1, p. 11, 2025.

[18] S. Hauert, S. Leven, M. Varga, F. Ruini, A. Cangelosi, J.-C. Zufferey, and D. Floreano, "Reynolds flocking in reality with fixed-wing robots: communication range vs. maximum turning rate," in *IEEE/RSJ international conference on intelligent robots and systems*, 2011, pp. 5015–5020.

[19] S. A. Quintero, G. E. Collins, and J. P. Hespanha, "Flocking with fixed-wing uavs for distributed sensing: A stochastic optimal control approach," in *IEEE American Control Conference*, 2013, pp. 2025–2031.

[20] M. Turpin, N. Michael, and V. Kumar, "Decentralized formation control with variable shapes for aerial robots," in *2012 IEEE international conference on robotics and automation*, 2012, pp. 23–30.

[21] C. Toumeh and D. Floreano, "High-speed motion planning for aerial swarms in unknown and cluttered environments," *IEEE Transactions on Robotics*, vol. 40, pp. 3642–3656, 2024.

[22] L. Bartolomei, L. Teixeira, and M. Chli, "Fast multi-uav decentralized exploration of forests," *IEEE Robotics and Automation Letters*, 2023.

[23] J. Tordesillas and J. P. How, "Mader: Trajectory planner in multiagent and dynamic environments," *IEEE Transactions on Robotics*, vol. 38, no. 1, pp. 463–476, 2021.

[24] E. Soria, F. Schiano, and D. Floreano, "Predictive control of aerial swarms in cluttered environments," *Nature Machine Intelligence*, vol. 3, no. 6, pp. 545–554, 2021.

[25] J. Park, Y. Lee, I. Jang, and H. J. Kim, "Decentralized trajectory planning for quadrotor swarm in cluttered environments with goal convergence guarantee," *The International Journal of Robotics Research*, pp. 1336–1359, 2025.

[26] M. Boldrer, P. Bevilacqua, L. Palopoli, and D. Fontanelli, "Graph connectivity control of a mobile robot network with mixed dynamic multi-tasks," *IEEE Robotics and Automation Letters*, vol. 6, no. 2, pp. 1934–1941, 2021.

[27] V. Walter, N. Staub, A. Franchi, and M. Saska, "Uvdar system for visual relative localization with application to leader–follower formations of multirotor uavs," *IEEE Robotics and Automation Letters*, vol. 4, no. 3, pp. 2637–2644, 2019.

[28] S. Lloyd, "Least squares quantization in pcm," *IEEE transactions on information theory*, vol. 28, no. 2, pp. 129–137, 1982.

[29] J. Cortes, S. Martinez, T. Karatas, and F. Bullo, "Coverage control for mobile sensing networks," *IEEE Transactions on Robotics and Automation*, vol. 20, no. 2, pp. 243–255, 2004.

[30] V. Walter, M. Vrba, D. B. Licea, M. Hilmer, and M. Saska, "Distributed formation-enforcing control for uavs robust to observation noise in relative pose measurements," *arXiv preprint arXiv:2304.03057*, 2023.

[31] T. Baca et al., "The mrs uav system: Pushing the frontiers of reproducible research, real-world deployment, and education with autonomous unmanned aerial vehicles," *Journal of Intelligent & Robotic Systems*, vol. 102, no. 1, p. 26, 2021.

[32] S. Kohlbrecher and J. Meyer, "Hector slam: A flexible and high-performance slam system for mobile robots," https://wiki.ros.org/hector_mapping, 2013.